DELFT UNIVERSITY OF TECHNOLOGY

MASTER THESIS

MASTER THESIS

Author:
Serwan Asaad

Supervisor:
Dr. Alessandro Bruno

May 25, 2015

Contents

INTRODUCTION

The subject of my Master's thesis will be on ways of improving T1 and T2 coherence times for qubits. The past few months I have been learning about superconducting circuit quantum electrodynamics. I have learned what set-ups are used for performing measurements on cQED samples, and about the types of measurements that are performed.

Traditionally the measurements were performed using Labview software. However, in the months that I have been working in the DiCarlo lab, a transition in measurement software has taken place from Labview to the Python-based QTLab. I have been very involved in this transition, as an important part of my research will be to characterize a sample quickly and accurately. This will enable a fast cycle from sample fabrication to characterization, hopefully leading to rapid progress in the development of quantum computing using cQED.

The past few weeks the focus of my measurements has shifted towards the characterization of resonators. This is largely due to the fact that two of my colleagues, Alessandro Bruno and Gijs de Lange, are working on a paper on ways of improving the quality factor of resonators. A large part of the data was already obtained before I joined the group, but a last set of measurements was required using the dilution refrigerator I most often operate at. The reason is that its base temperature is at 15 mK, which is considerably lower than the base temperature of the refrigerator at which the other measurements were performed, namely 250 mK. Because my focus so far has been more on resonators than on qubits, the main topic of this report will be on resonators, and I will include the topic of qubits in my final thesis.

Because the relevant regime where resonators interact with qubits is the single-photon regime, a very weak signal must must be applied to determine its properties in that regime. At this point noise becomes a relevant issue. I will therefore also devote a section of this report on the subject of noise.

Part I

Resonators

When a signal enters a fridge it is attenuated in several stages and eventually reaches the sample being measured. In the sample the signal travels through a feedline. One or more resonators can then be capacitively coupled to the feedline. Qubits can then also be capacitively coupled to the resonators, and a resonator can even be used to connect qubits, in which case the resonator is known as a 'bus'. However in this report only resonators connected to a central feedline will be discussed.

0.1 COPLANAR WAVEGUIDE

In the context of circuit QED, one of the most common types of resonators are coplanar waveguides (CPW). Coplanar waveguides consist of a long central conducting track, with on both sides a neighbouring grounded track. The conducting track is seperated from the grounded tracks by a fixed distance.

One end is usually capacitively coupled to a feedline and has an open end, while the other end can either be open or shorted. This determines whether the resonant frequencies have a node or an antinode at that end. In the case of a shorted end, the resonant frequencies have an antinode at that end, resulting in a quarter wave resonator. This means that the wave-

Figure 1: Schematic of a coplanar waveguide.

length of the fundamental mode fits a quarter times into the resonator. In the case of an open end, the resonant frequencies have an node at that end, resulting in a half wave resonator.

0.2 QUALITY FACTOR

The quality of a resonator can be quantified through its quality factor. Generally speaking, the quality factor of a resonator determines the ratio between energy stored in a resonator and the energy leaking away from the resonator. For cQED resonators this corresponds to the rate at which photons dissipate from the resonator. A high quality factor corresponds to a low dissipation rate.

The quality factor can also be defined in two different ways [7, p. 23-24]:

$$Q = \omega_0 \tau_1 = \omega_0 / \Delta\omega \tag{1}$$

Here ω_0 is the resonance frequency of the resonator, and τ_1 is the decay time of the resonator. The decay time is the time taken by a resonator to dissipate its energy to $1/e$ of its original energy. One can see that this definition is in accordance with the first definition, as the energy is related to frequency through the Planck-Einstein relation: $E = \hbar\nu$, and therefore increases with increasing frequency.

Photons can dissipate from the resonator through the resonator's different loss channels. Each of these loss channels has a corresponding quality factor. One such loss channel is due

to resonators in cQED being capacitively coupled to a feedline. The quality factor associated to this loss channel is known as the coupling quality factor Q_c. This coupling quality factor depends on the amount of capacitive coupling between the resonator and the feedline. It can therefore be engineered to have a certain value, depending on the amount of interaction wanted between resonator and feedline.

The other loss channels are usually unwanted, and therefore desired to be as low as possible. These individual channels are usually lumped together, resulting in a combined quality factor, known as the intrinsic quality factor Q_i.

The total quality factor of the resonator is known as the loaded quality factor Q_l. It is related to Q_c and Q_i through:

$$\frac{1}{Q_l} = \frac{1}{Q_c} + \frac{1}{Q_i} \tag{2}$$

From equation 2 it can be seen that if the difference between Q_c and Q_i is large, then the loaded quality factor Q_l will be approximately equal to the minimum of the two.

For a quarter wave resonator the amplitude of transmission has a minimum S_{21}^{min}, given by [7, p. 29]:

$$S_{21}^{min} = \frac{Q_c}{Q_c + Q_i} \tag{3}$$

With knowledge of the resonant frequency ω_0, the resonant width $\Delta\omega$, and the transmitted signal at resonance S_{21}^{min}, it is possible through equations 1 and 3 to determine both the coupling quality factor Q_c and the intrinsic quality factor Q_i. Note that as equation 3 depends on the ratio of the two quality factors, to get an accurate estimate of both quality factors, they should have a comparable value.

One reason why a high quality factor is important in the context of cQED is that a qubit can be coupled to a resonator. This qubit therefore experiences dissipation due to its coupling to the resonator, known as the Purcell effect. The result of dissipation is that when the qubit is in its excited state, it will relax to its ground state. The amount of relaxation due to the Purcell effect can be quantified through its relaxation time T_1^{Purcell}. The reason a high quality factor is important is because the Purcell relaxation time is proportional to the quality factor [5, p. 22]. The Purcell relaxation time T_1^{Purcell} places an upper limit on the relaxation time T_1 of a qubit. If the qubit's relaxation time T_1 is close to this value, the qubit is said to be Purcell limited.

0.3 LOSSES

When a resonator is being driven at its resonance frequency, it is absorbing photons from the external source. When this external driving stops, the resonator slowly loses its photons through its different loss channels.

One loss channel has already been discussed in section 0.2, namely through the coupling to the feedline. This loss channel is not unwanted, as the amount of coupling to the feedline determines how fast the resonator and feedline can interact with each other. The other loss channels, however, are unwanted. They cause dissipation of energy, and hence information. Some of the main causes of loss will be discussed in this section.

0.3.1   Causes of loss

0.3.1.1   Two-level systems

Two-level systems (TLS) are systems which can be in a ground state or in an excited state. In some cases they can be useful. In fact a qubit itself is an example of a TLS. In other cases, however, TLS can also be a source of dissipation such as in the case of dielectric loss [6]. Study suggests that in cQED, most TLS reside in a thin oxide layer at the metal-substrate interface and the substrate-air interface [15].

Resonators are surrounded by a large quantity of TLS, each of which has its own resonance frequency, depending on its energy landscape. When the resonance frequency of a TLS is close to that of the resonator, it can absorb a photon from the resonator, upon which it tunnels to an excited meta-stable state. TLS have a finite lifetime in their excited state, after which they decay back to their ground state and are then again able to absorb a photon. The rate at which a TLS absorbs a photon depends on the electric field surrounding the TLS.

In the low power, low temperature regime, TLS reside mostly in their ground state, and only occasionally tunnel to the excited state, upon absorption of a photon. It is theorized that, in this regime, TLS are the main source of dissipation for resonators [4]. At higher powers and/or temperatures, TLS will tunnel to an excited state at a higher rate. Due to their finite lifetime they become saturated at a certain point. Since the quality factor depends on the ratio between energy stored and energy dissipated, when the TLS are saturated the amount of dissipation is limited, while the energy stored in the resonator can still increase. Therefore, in the low power, low temperature regime, increasing either of the two parameters results in an increase in quality factor. At a certain point, however, further increasing either of the two will not improve the quality factor. This is due to other effects dominating the dissipation rate in these regimes.

0.3.1.2   Quasiparticles

Another source of dissipation for resonators is due to quasiparticles being present in the superconducting layer. When a Cooper-pair is broken up, Bogoliubov quasiparticles are formed [2, p. 16]. Once formed, the quasiparticles have a finite lifetime, depending on the temperature of the system. These quasiparticles can have either electron-like or hole-like properties. They are a source of dissipation for resonators, since they are non-superconducting and therefore cause the surface impedance to be slightly resistive [7, p. 18].

The breaking up of Cooper-pairs is due to excitations. These excitations can either be thermal, or due to photon absorption. Therefore an increase in temperature or an increase in photon density will result in a higher density of quasiparticles. The quasiparticle density increases exponentially with increasing temperature [7, p. 44].

0.3.1.3   Radiation

A third source of dissipation is due to radiation from the resonator. This radiation is due to the spontaneous emission of photons.

The amount of dissipation due to radition is directly related to the geometry of the resonator through [12, 7]:

$$Q_{\text{rad}} = \alpha \left(\frac{L}{s + w} \right)^{n_r} \tag{4}$$

As shown in Figure 1, s is the distance between the conducting and grounded track, w is the width of the conducting track, and L is the length of the resonator. The parameter α depends on properties such as impedance and the dielectric constant of the substrate, and n_r depends on the shape of the resonator, and is equal to 2 in the case of a straight resonator. From Formula 4 it is clear that a decrease of the conducting track width or the distance between tracks leads to an increase in Q_{rad}. However, with a decrease of either of the two parameters, the field strength close to the resonator becomes higher. If the TLS are not saturated (i.e. low power and temperature), this will increase the amount of dissipation through TLS. Therefore it is not necessarily advantageous to minimize s and w.

Radiation loss becomes the dominant source of dissipation at high powers and/or temperatures, but otherwise usually is not the limiting factor. Since measurements relevant for quantum computing are usually operated at low power and temperature, this source of dissipation is usually less important than other sources, such as TLS dissipation.

0.3.1.4 Vortices

When a sample is cooled down to a superconducting state there may still be a small, but nonnegligible magnetic field present. The presence of a magnetic field can cause vortices to appear in superconducting materials. These vortices have a non-superconducting core. Current passing through superconductive material exerts a Lorentz force on vortices. For a resonator being driven on resonance, this AC current results in the vortices near the resonator experiencing a dissipative oscillatory motion [10].

It is interesting to note that the presence of vortices does not necessarily lead to a lower internal quality factor. The influence of a vortex on a resonator depends on its location. As reported by Nsanzineza et al. [9], a vortex close to a current antinode of a resonator, can result in a significant loss of the quality factor. A vortex close to a current node, however, may even increase the quality factor of the resonator. They attribute this increase in quality factor to quasiparticles, which would otherwise lead to dissipation, being trapped in the vortex.

0.3.2 Minimizing losses

0.3.2.1 Surface treatment

Previous research has determined that for resonators, TLS are mostly present at the surfaces [4]. These oxides may reside at the interface between metal and dielectric, or between the dielectric and vacuum, or possibly between metal and vacuum (depending on the type of metal used). One explanation for TLS being present is the presence of an amorphous oxide layer at the interfaces. These oxides may act as TLS. During deposition of the metal on the dielectric, this oxide layer can become trapped between the two interfaces. For a silicon

dielectric, this oxide layer can be removed by shortly treating the sample with hydrophluoric acid. This process is also known as an 'HF dip'.

Aside from the HF dip, additional surface treatment can be applied. For the resonators measured in this report, before depositing the metal on the substrate, an additional exposure to hexamethyldisilazane (HMDS) was applied. The reason for this additional step is that there is a lattice mismatch between the metal and substrate. The intermediate layer of HMDS can possibly mediate this lattice mismatch. See [3] for more information.

0.3.2.2   Infrared shielding

Aside from thermal excitation, quasiparticles are also formed from the absorption of photons. High-frequency photons (UV-range or higher) are usually not a significant contribution, as they are easily absorbed by materials, well before they reach the inner layers of the fridge. Lower-frequency photons, such as in the infrared range, however, can penetrate through the fridge to the sample. These infrared photons can cause the excititation of quasiparticles. By using infrared shielding, such as a coating film inside the fridge, the amount of infrared radiation reaching the sample can be lowered.

0.3.2.3   Deep-reactive ion etching

Another technique applied to the resonators studied in this report is deep-reactive ion etching (DRIE), which is a type of Bosch process [3]. In this technique two alternating steps are performed:

1. An etching step in which an SF_6 plasma is used to etch the substrate layer.

2. A passivation step in which C_4H_8 is released. The gas forms a protective layer on the substrate, except for the direction in which the etching plasma is accelerated. The result is that the sidewalls are protected from the etching process

Using DRIE, nearly vertical sidewalls can be created for the substrate. The result is that the substate-air interface is removed from the regions between the CPW tracks, which are the regions where the electric field strength is high. As the dissipation due to TLS depends on the electric field strength, it is expected that DRIE will result in a lower TLS dissipation rate at this interface.

0.3.2.4   Magnetic shielding and vortex trapping

Vortices are created when a magnetic field is present. One method to lower the amount of vortices is to use proper magnetic shielding around the sample. Furthermore, using nonmagnetic materials also result in lower amounts of vortices being present.

Even when using these methods to counter the presence of magnetic fields, there may still be a small amount of vortices present in the sample, which may lead to dissipation. To counter their movement a grid-like structure can be added in the superconducting material, effectively pinning the vortices.

0.4 EXPERIMENTAL SET-UP

The fridge used in this experiment is a dilution refrigerator, made by Leiden Cryogenics. The refrigerator has a base temperature of ~15 mK. An input signal was generated using a Rohde & Schwarz ZVM vector network analyzer, connected to an Aeroflex 8310 step attenuator, which has an attenuation range of 120 dB. The signal out of the fridge was measured using the same vector network analyzer.

Figure 2: Optical microscopy image of the sample measured in this report. The sample consists of ten quarter wave resonators, with frequencies ranging between 1–11 GHz, connected to a central feedline. The resonators are made using NbTiN on a Si substrate. The sample is treated with HMDS and DRIE.

Using this set-up, quarter wave resonators, fabricated by Alessandro Bruno, were measured in a frequency range between 1–9 GHz. The sample is shown in Figure 2. The resonators were made using NbTiN on a silicon substrate. The advantage of NbTiN is that the metal atoms are bound to nitrogen, thereby inhibiting bond formation with oxides. In a way to minimize losses, all resonators were treated with HMDS and deep-reactive ion etching.

By driving a signal through the feedline, the resulting transmitted signal S_{21} can be measured. At or close to the resonance frequency of a resonator, the resonator will either cause enhanced transmission (half wave resonator), or diminished transmission (quarter wave resonator).

Unless stated otherwise, all measurements were performed with the fridge at base temperature (~15 mK).

0.5 RESULTS AND DISCUSSION

0.5.1 Resonator measurement

In Figure 3 the transmission S_{21} of a resonator is shown. Figure 3(a) shows the transmitted voltage $|S_{21}|$ of the resonator as a function of frequency. As one can see, the resonator has a shape similar to a Lorentzian dip. One interesting point is that the Lorentzian exhibits an asymmetry, which is often attributed to reflections in the feedline [5, p. 192]. This could be caused by impedance mismatching.

0.5.2 Power dependence

To be able to study the behaviour of the resonators, measurements were performed for several powers. Using proper calibrations for the attenuation down to the sample, the power can be converted to the input power at the sample. This value can then be converted to the mean number of photons present in the resonator [3]. The results are shown in Figure 4.

Figure 3: Forward transmission S_{21} spectrum of a resonator around 2.75 GHz. Panel (a) shows the amplitude of S_{21}, along with a fit (red). Panel (b) shows the path of S_{21} in the complex path, along with a fit (red). The green dot indicates the resonance frequency of the resonator. Measurement was performed at 15 mK at an input power of -123 dBm corresponding to $\sim 5 \times 10^4$ photons.
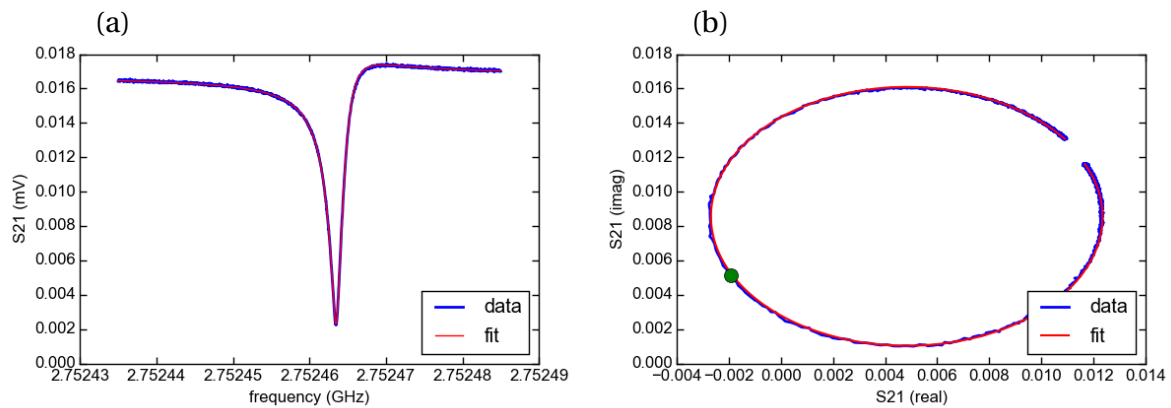
As can be seen, the internal quality factor Q_i of all resonators decrease with decreasing photon number. One explanation for this phenomenon is that the dissipation dissipation is mainly due to TLS. Since measurements were performed at ~15 mK, the TLS are not saturated since the rate of thermal excitation is low. As discussed in section 0.3.1.1, the relative loss due to TLS is highest at low power, in the regime where they are not saturated. Therefore the fact that the internal quality factor Q_i rises with the mean number of photons present in the resonator can be attributed to a larger amount of TLS being satured. This would suggest that, even with HMDS and DRIE treatment of the sample, at low power and temperature, the internal quality factor is still limited by TLS being present.

The mean photon number of a resonator is inversely proportional to the square of frequency [3], so for resonators with a low frequency a lower input power is required than with a high frequency. At high photon numbers this is not a concern, as the transmitted signal is high enough to be accurately measured in a short period of time. For the single-photon powers, however, which is the region of interest for quantum computation, acquiring enough signal took up to five hours for the lowest frequencies. The reason that for the resonator with a resonance frequency at 1.83 GHz has large error bars at low powers can be partly attributed to this, but as we will see in section A.4, the main reason is that its frequency lies outside the bandwidth of the amplifiers and circulators of the set-up, resulting in a large amount of additional noise.

0.5.3 Temperature dependence

Aside from power, some of the dissipation channels also depend on the temperature of the system. To be able to study the effect of temperature on resonators, the resonator with frequency 2.75 GHz has been studied as a function of power for several temperatures ranging from 15 mK up to 400 mK. The reason for choosing this resonator is that it has the highest internal quality factor of all the resonators measured, and so any change in quality factor
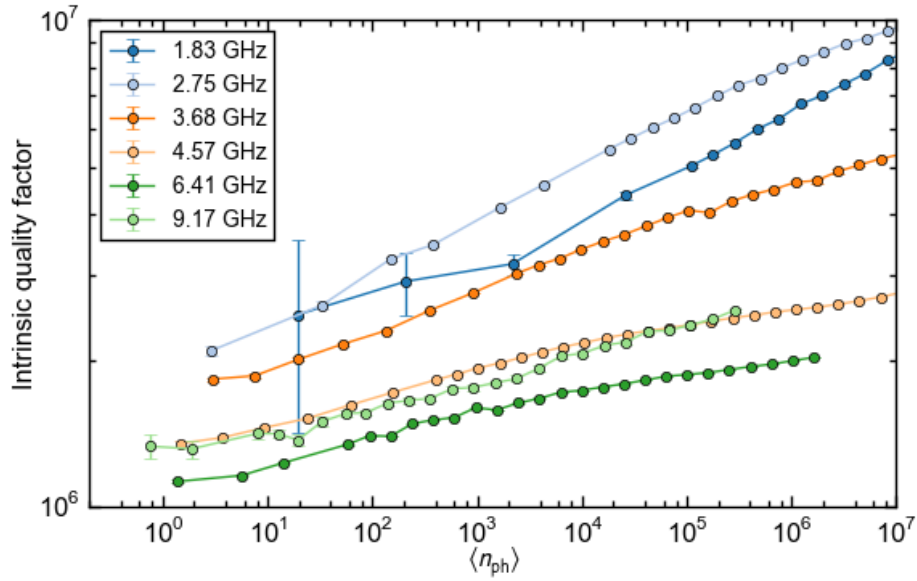
Figure 4: Intrinsic quality factor of resonators as a function of mean number of photons present in the resonator. Measurements were performed at 15 mK.
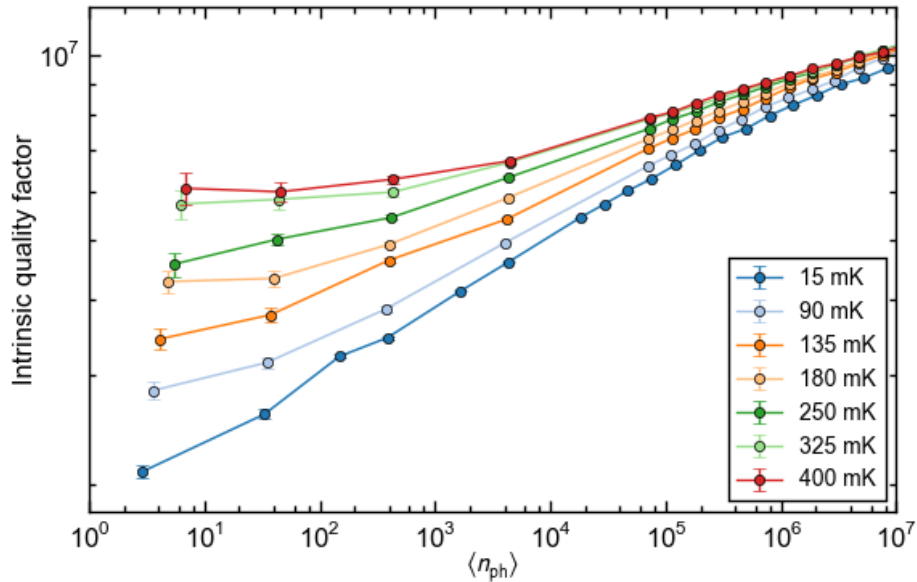

Figure 5: Intrinsic quality factor versus photon number for temperatures ranging from 15 mK up to 400 mK. All measurements were performed for a resonator with resonance frequency f_0 =2.75 GHz.

would be most clearly visible.

The results are shown in Figure 5. As can be clearly seen, the quality factor increases with increasing temperature. This is likely due to the fact that TLS are thermally excited for a larger percentage of time. Therefore, the relative energy dissipation with respect to total energy in the resonator will be lower, resulting in an increase in quality factor.

Another interesting point is that the increase in quality factor as a function of temperature is largest at low powers. This can also be explained when the limiting factor is due to TLS. With low powers, the TLS are almost exclusively excited thermally, while at higher powers, the excitation of TLS is not only due to thermal excitations, but also from photon absorption.

If one looks at the highest temperatures, it seems that the increase in quality factor as a function of temperature seems to slowly approach a saturation point. One reason is that the TLS are approaching their saturation, and so increasing the temperature further will have little effect on the percentage of time that the TLS are in the excited state. As will be shown in the next section, at 400 mK the quality factor of the resonator is close to its maximum value, and will decrease as temperature is further increased.

0.5.4 Temperature tracking
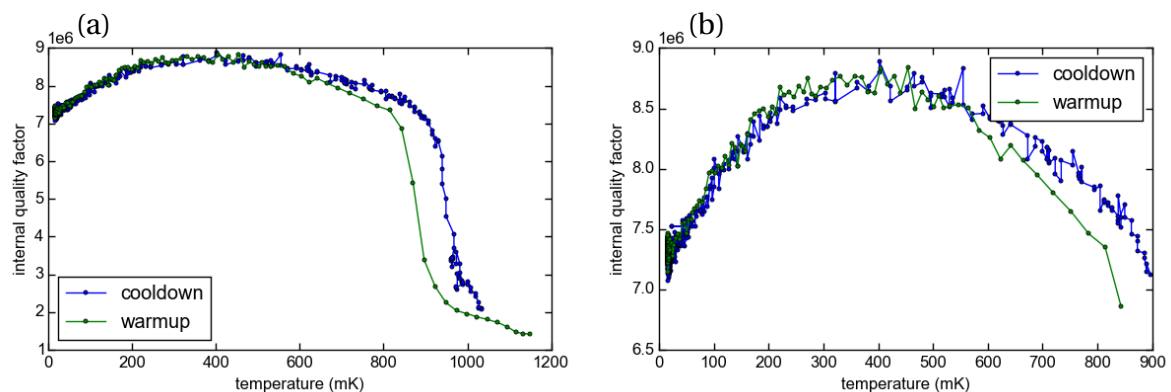
Figure 6: Internal quality factor versus temperature for the resonator with resonance frequency f_0 =2.75 GHz. Quality factor was continuously measured as the sample was cooled down and warmed up four days later. Panel (a) shows the full temperature range up to the helium condensation cycle. Panel (b) shows a close-up of the region until 900 mK.

To further investigate the temperature dependence of the resonator, a continous measurement was performed on the resonator with resonance frequency 2.75 GHz during a cool-down and a subsequent warm-up of the fridge four days later. Measurements were performed for temperatures ranging from base temperature (15 mK) to roughly 1 K. Above this temperature, the fridge entered a cyclic helium condensation/evaporation process. All temperatures were measured at an input power of −113 dBm, corresponding to roughly 5×10^5 photons. In Figure 6 the internal quality factor versus temperature is shown during a cooldown and subsequent warm-up of the fridge. As can be seen, the quality factor reaches a maximum quality factor at a temperature of ~400 mK. Below this temperature, the quality factor is likely

limited by the presence of TLS (see sections 0.5.2 and 0.5.3). Above this temperature however, the quality factor decreases, indicating that TLS are not the limiting factor anymore for Q_i. One likely explanation is that the main source of dissipation is now due to the presence of quasiparticles in the resonator. At even higher powers other effects, such as vortices and enhanced radiation, contribute more and more significantly to the decay of the quality factor.

From Figure 6 it seems that there is some hysteresis at high temperatures. However, this is likely due to the fact that the thermometer is at a different position in the fridge as the sample, and does not thermalize equally fast. There may therefore be a delay between the temperature of the thermometer, and the actual temperature of the sample.
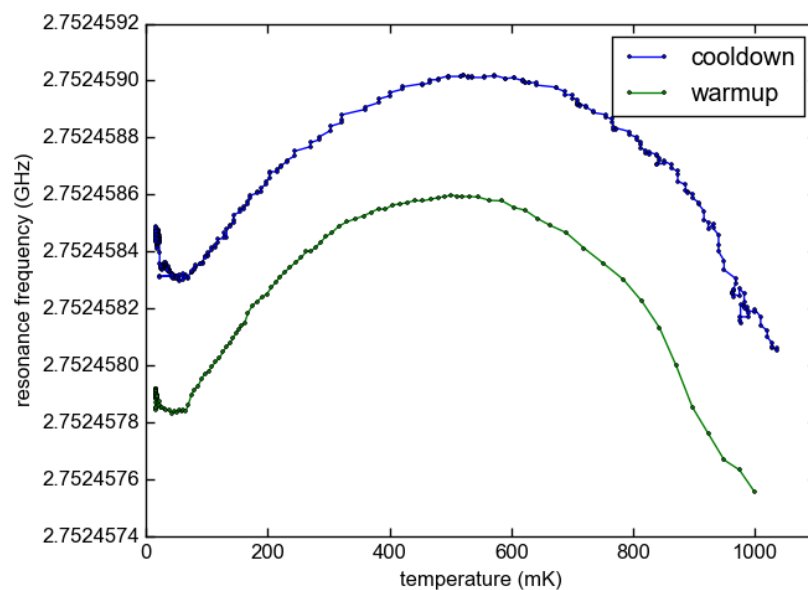
Figure 7: Resonance frequency versus temperature during a cooldown and subsequent warm-up four days later. In the period between cooldown and warm-up the resonance frequency has shifted by ∼500 Hz, possibly due to phase noise.

Aside from the internal quality factor, another quantity of interest is the resonance frequency f_0 of the resonator, which also depends on the temperature. The result from of tracking the resonance frequency of the resonator during cooldown and subsequent warm-up is shown in Figure 7. As can be seen in both cases, the resonance frequency reaches a maximum around 500 mK.

Between the cooldown and warm-up the resonance frequency seems to have shifted by roughly 500 Hz. As the sample was kept at 15 mK, it is unlikely that this decrease in resonance frequency is due to degradation of the sample. One possible explanation is that this change in resonance frequency is due to phase noise, which is known to shift the resonance frequency of the resonator. Further measurements are, however, required to determine if this is the case.

The decrease in resonance frequency at higher temperatures can be explained by the presence of quasiparticles, which increase the kinetic inductance [5, p. 91]. The resonance

frequency is inversely proportional to the square root of the total conductance [1], and so an increase in kinetic inductance leads to a decrease in resonance frequency. For measurements done by Barends et al. [1], the change in resonance frequency due to changes in the kinetic inductance seem to roughly correspond with the decrease in center frequency measured in Figure 7.
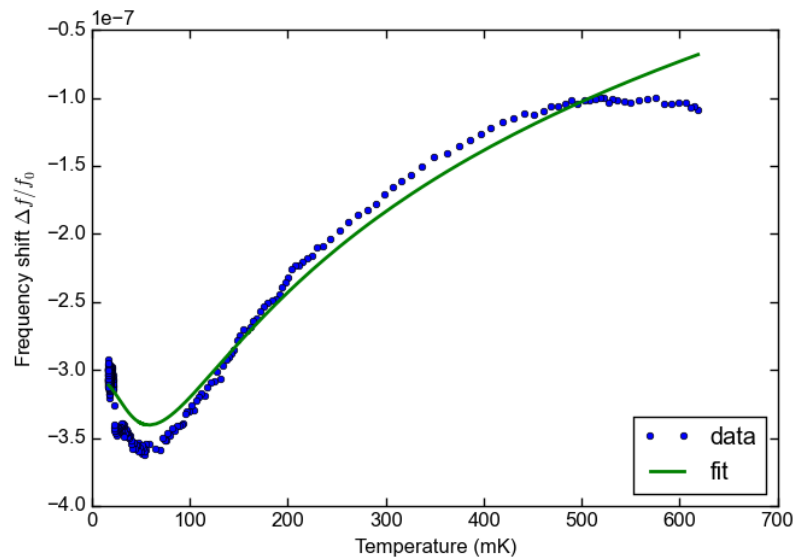
Figure 8: Frequency shift versus temperature for low temperatures, along with fit (green). The fit was performed using the model by Gao et al. [4]. The fit corresponds well with data, even describing the frequency peak at the lowest temperatures.

The decrease in resonance frequency at lower temperatures can be explained due to TLS still being present. A model is presented by Gao et al. [4], in which they describe the decrease in resonance frequency due to the presence of TLS. As can be seen in Figure 8 the model corresponds well with the data at low temperatures. At higher temperatures the model deviates from data, which may be explained by quasiparticles dominating as source of dissipation. An interesting thing to note is that an increase in resonance frequency was predicted at the lowest temperatures, but as they did not reach temperatures sufficiently low they could not confirm this effect. In Figure 8 however, this increase in resonance frequency is observed. This supports the claim that at low temperatures the resonator is still limited by TLS, even after treatment of HMDS and DRIE.

0.6   CONCLUSION AND FUTURE WORK

Since the quality factor of all resonators is found to decrease with decreasing input power, this indicates that at low temperatures and powers the limiting factor is still due to TLS. The fact that the quality factor initially increases with higher temperatures, supports this claim. By also measuring the resonance frequency as a function of temperature, the curve obtained is

in good agreement with a model describing the resonance frequency shift due to TLS [4]. The curve even shows an increase in resonance frequency at the lowest temperatures, which was also predicted by the model. These results suggest that even after HMDS surface treatment and deep-reactive ion etching was applied, the internal quality factor of the resonator at low temperatures and power is still limited by the presence of TLS.

Nevertheless, As shown by Bruno et al. [3], the application of HMDS surface treatment and DRIE resulted in an improvement of the internal quality factor of the resonators by almost an order of magnitude. More research must be done to determine at what interface the dissipation due to TLS is greatest after these two treatments.

The next step is to perform the same treatments (HMDS and DRIE) on transmon qubits, to study what the influence will be on coherence times.

Part II

Muxmon experiment

large TODO:

- Explain surface code architecture

- Explain the general structure of a chip:

    - Feedline through which signal is sent and measured
    - CPW resonators, capacitively coupled to feedline
    - Single qubit coupled to resonators (coupling location?)
    - Resonator buses

small TODO:

- Rename DAC voltage to flux, and mention early on that this renaming will be used

- flux-bias line or flux bias line?

Introduction

At this moment circuit QED is at the stage where multi-qubit experiments are being realized.

Chapter 1

Muxmon chip architecture

Topics that should be explained in this section:

- The Muxmon0 and Muxmon1 chip are designed with two purposes
    1. Testing multiplexing using the Duplexer
    2. Explore qubit frequency re-use
- Explain similarities of chips
    - Three qubits per chip
    - All three qubits have individual flux tuning
    - Air bridges are used, not only for connect the ground planes, but also such that the feed line can pass over other coplanar waveguides without contact

- Explain differences between Muxmon0 and Muxmon1.
    - The Muxmon0 chip has a driving line connected to each of the qubits.
      It has two resonator buses at 4.9 GHz and 5.0 GHz.
      These could also be used for two-qubit gates.

        Advantage Able to fully control each qubit individually, even when multiple qubits share the same frequency.

        Advantage Less coupling between data qubits.

        Disadvantage Requires more driving lines.

        Disadvantage Adds extra source of dissipation for the qubits.

    - The Muxmon1 chip has two driving lines, each capacitively coupled to one of the two data qubits, and to the ancilla qubit.

        Advantage Less driving lines required

        Advantage Less dissipation due to capacitive coupling

> **Disadvantage** Cannot individually control data qubit and ancilla qubit when
> they share the same frequency
>
> **Disadvantage** More coupling between qubits
>
> – Simplified model of the surface code

- Explain concepts of cross-coupling and readout cross-talk

> **Cross-coupling** The coupling between qubits.
> Cross-coupling leads to transfer of excitation.
> An associated coupling strength **g** can be associated to cross-coupling.
> Can be determined by driving one qubit extremely hard, and measuring signal
> from other qubit.
> **TODO:** Show values of cross-coupling found, or do this in characterization section
> **TODO:** Leads to coherent errors?
> **TODO:** Two types of cross-coupling? Direct leakage of pulse pulse, and transfer of
> excitation? cross-driving?
>
> **Readout cross-talk** Coupling between a qubit and a resonator that are not directly
> coupled.
> A part of the signal measured from one resonator is then due to the state of another
> qubit
> **TODO:** Understand more behind readout cross-talk

Left to think about:

- Should I already include items such as coherence times, the fact that Muxmon0 performs better than Muxmon 1?

- Where should I include coherence times versus frequency?

- Should the part on cross-coupling and readout cross-talk not be in characterization section?

- Should the section on the Duplexer go in here?

Figures that need to be included:

- Muxmon0 and Muxmon1 chip, preferably optical microscopy

- SEM image of air-bridges such that coplanar wave-guides cross without intersecting

- schematic of cross-coupling and readout cross-talk
  It could be good to create this using the actual Muxmon chip as background, with
  arrows indicating how the different effects operate

Chapter 2

Qubit characterization

Description This chapter gives a step-by-step description of how to find a resonator and qubit, and subsequently how to tune the qubit's parameters.

In the design of cQED chips, the parameters of the qubits and resonators are always targeted which are ideal for the experiment. For coplanar waveguide resonators one can already obtain relatively good parameters for the required dimensions from simple formulae **TODO:** refer to formula. For superconducting transmon qubits, however, finding the right dimensions that correspond to the desired parameters is a much more complicated process. The qubit's frequency, for instance, depends on the qubit's coupling energy E_c and Josephson energy E_J. The coupling energy E_c can be reasonably estimated from classical simulations. Finding the right dimensions for the Josephson junction that result in the desired Josephson energy E_J, however, is difficult, and usually physically testing different junctions is necessary to determine an accurate conversion from the desired E_J to the Josephson junction dimensions.

Nevertheless, the actual parameters of the resonators and qubits are almost never where one expects them to be. Once the sample is cooled in the dilution refrigerator, an inevitable game of hide-and-seek follows with the goal of finding the frequency of the resonators and qubits, and subsequently determining their properties. This chapter describes the measurements that were performed to characterize the MuxMon samples.

2.1 CONTINUOUS-WAVE MEASUREMENTS

Once a sample is properly cooled down it is ready to be measured. At this stage the sample is still an unknown terrain, where the experimenter only has a rough map, containing the sample's targeted parameters, and the specific properties of the resonators and qubits.

The first step is to look for signs of life. These manifest themselves as resonance frequencies of the resonators and the qubits that are coupled to them. As we are not yet interested in the properties of the resonators and qubits which can only be obtained through measurements with accurately timed pulses, we send continuous tones through the feedline, and measure deviations in the transmission. These measurements are known as continuous-wave measurements

2.1.1 Scanning for resonators

Since communication with the qubits is mediated through their coupling to resonators, the first step is to find these resonators. This is done using a transmission measurement, in combination with heterodyne detection, and has been explained in section **TODO:** Create section in Resonator chapter.

There is one difference in measuring a resonator when there is a qubit coupled to it. When considering the qubit as a two-level system, the behaviour of the coupled resonator-qubit system is governed by the Jaynes-Cummings Hamiltonian [11]:

$$\hat{H} = \hbar\omega_\mathrm{r}\left(\hat{a}^\dagger\hat{a} + \frac{1}{2}\right) + \frac{\hbar\omega_\mathrm{q}}{2}\hat{\sigma}_z + \hbar g\left(\hat{a}^\dagger\sigma_- + \hat{a}\sigma_+\right) \tag{2.1}$$

where ω_r is the bare resonance frequency of the resonator, ω_q is the resonance frequency of the qubit's ground to excited state transition, and the qubit's two states are in the spin-representation. This Hamiltonian consists of three terms. The first term corresponds to the energy level of the resonator, the second to the energy level of the transmon, and the third is a coupling term between the two with coupling strength g.

The difference between the resonator's frequency ω_r and the qubit's frequency ω_q is given by the detuning $\Delta = \omega_\mathrm{q} - \omega_\mathrm{r}$. If the magnitude of the detuning is large compared to the coupling strength g, the system is in the dispersive regime. In this case the Hamiltonian can be approximated by the dispersive Jaynes-Cummings Hamiltonian:

$$\hat{H} = \frac{\hbar\omega_\mathrm{q}'}{2}\hat{\sigma}_z + \left(\hbar\omega_\mathrm{r}' + \hbar\chi\hat{\sigma}_z\right)\hat{a}^\dagger\hat{a} \tag{2.2}$$

The coupling between the qubit and resonator causes both qubit's frequency and the resonator's frequency to shift: $\omega_\mathrm{q}' = \omega_\mathrm{q} + \chi_{01}$, $\omega_\mathrm{r}' = \omega_\mathrm{r} - \chi_{12}/2$.

Aside from experiencing a frequency shift dependent on the amount of detuning, Equation 2.2 shows that the resonator also experiences a shift depending on the state of the qubit. The resonator's frequency is decreased by an amount 2χ when the qubit is in the excited state. The parameter χ is the dispersive shift, and is given by:

$$\chi = \chi_{01} - \chi_{12}/2 \approx \frac{g^2}{\Delta}\frac{E_\mathrm{c}}{\hbar\Delta - E_\mathrm{c}} \tag{2.3}$$

where $\chi_{ij} = \frac{g_{ij}^2}{\omega_{ij} - \omega_c}$ are the partial dispersive shifts.

Due to this coupling between resonator and qubit, it is important to choose the right RF power. When the amount of photons in the resonator reaches a certain point, this coupling will result in the resonator experiencing nonlinear effects. The resonator will thereby lose its Lorentzian lineshape. Therefore the RF power should be kept sufficiently low to avoid these nonlinear effects, while still maintaining a good signal-to-noise ratio.

TODO:

- In the strong coupling regime (Leads to hybridization of qubit and resonator states: quton and fobit

- Explain that the quality factor is low because the resonator is coupled strongly to the qubit (equation including coupling to qubit?)

- Doesn't χ diverge when $\Delta \rightarrow E_c$?

- explain concept of anharmonicity, and that $\alpha \approx E_c$

- Maybe explain concept of number splitting in dispersive Jaynes-Cummings. Number splitting is the phenomenon that the qubit's frequency shifts by an amount 2χ for every photon in the resonator.
  Alternatively mention this in another section.

- Mention that $g_{12} = \sqrt{g}$, and that other coupling strengths are exponentially suppressed in the transmon

Figures:

- Figure of transmission showing all three Muxmon0 resonators

2.1.2   Powersweeping the resonators

Once the resonators have been located, the next stage is to find the qubit that is capacitively coupled to each of the resonators. Instead of directly scanning the entire frequency spectrum in search of the qubit, it is relatively straightforward to perform some initial measurements aimed at gaining information about our resonator and qubit, which will allow us to search for our qubit with much greater accuracy.

As explained previously, the capacitive coupling between the resonator and qubit shifts the resonator frequency ω_r from its bare frequency. When the amount of photons in the resonator reaches a certain point, the resonator experiences nonlinearity, thereby losing its Lorentzian lineshape. When increasing the RF power even further, at a certain point the resonator regains its Lorentzian lineshape. In doing so its resonance frequency has shifted to its bare frequency ω_{bare}. If this frequency shift is observed, it indicates that the resonator's frequency was shifted, and hence that the qubit is alive. Measuring this frequency shift is commonly done in a powersweep. A powersweep is a measurement in which a resonator scan is performed for a range of powers.

A powersweep additionally provides information about at what power the resonator enters the nonlinear regime. For measurements involving the qubit the readout power must be below this threshold power. Furthermore, from the frequency shift between the dressed cavity frequency and the bare cavity frequency, the amount of detuning between the qubit and the resonator can be estimated using Equation 2.3.

If no shift is observed, it could mean that the qubit is dead (e.g. because the Josephson junction is shorted). However, this is not necessarily the case. An alternative possibility is that the detuning between qubit and resonator is very large, and as a result the frequency shift cannot be discerned. At this point it is too early to draw conclusions, and we may almost draw the analogy with Schrödinger's cat in a box.
TODO:

- Explain theory behind transition to bare cavity frequency (Reed's thesis has some information)

Figures:

- Powersweep of ancilla qubit

2.1.3   Scan for qubit sweet-spots

Some of the qubits have a tunable resonance frequency. This is done through a superconducting quantum interference device (SQUID). In this case the two islands that compose the transmon qubit are connected by two Josephson junctions instead of one, effectively forming a loop. The SQUID loop is sensitive to the amount of flux passing through the loop. The amount of flux going through the SQUID loop can be changed by changing the surrounding magnetic field. This is commonly done by having a flux bias line in close proximity to the SQUID loop. Current flowing through the flux-bias line alters the magnetic field in the vicinity of the SQUID loop, and hence changes the amount of flux through the SQUID loop. A digital-to-analog converter is used to specify the amount of current that is sent through the flux bias line. Depending on the amount of flux through the SQUID loop, the resonance frequency of the qubit changes accordingly. these qubits are therefore called flux-tunable.

For qubits that are flux-tunable, finding the sweet-spot of the qubit can be done without knowledge of the qubit's frequency. This can be done by sweeping the DAC voltage and measuring the shift in the resonance frequency. Because the frequency of the qubit varies as the amount of current through the flux-bias line changes, the detuning between the qubit and the resonator consequently changes. As a result the dispersive shift χ, and therefore the resonator's frequency, also varies. At the sweet-spot of the qubit, the resonator's frequency ω_r is at a maximum. This is irrespective of whether the qubit's frequency ω_q is above or below the resonator's frequency.

The accurate way to measure the sweet-spot is to perform resonator scans as the DAC voltage is varied. The result is a 2D scan shown in **TODO:** Figure.

A faster second approach for finding the qubit sweet-spot, at the cost of providing less information, is by choosing a fixed frequency close to the resonator's frequency ω_r (preferrably slightly below, where the transmission slope is steepest). By measuring the amount of transmission as the DAC voltage is being varied, one obtains essentially a line-cut of **TODO:** Figure. The idea this measurement is that if the qubit's frequency f_q decreases, the resonator's frequency also decreases, resulting in a decrease in transmission (closer to ω_r). Likewise, if the qubit's frequency ω_q increases, the resonator's frequency increases **TODO:** Why?, resulting in an increase in transmission (further away from ω_r).

At the qubit's sweet-spot, the resonator's frequency ω_r is at a maximum, and so the transmission should also be at a maximum. Furthermore, because the amount of detuning only depends on the deviation from the flux sweet-spot **TODO:** improve, the transmission should be symmetric with respect to the DAC voltage sweet-spot. If the resonator's frequency ω_r shifts by a large amount in the course of this measurement, it becomes harder to determine where the sweet-spot is (although even then often it can still be discerned). Nevertheless,

this method is considerably faster than performing a full two-dimensional scan of frequency versus DAC voltage, and in most cases it works like a charm.

In the case where the powersweep showed no measurable frequency shift, these two measurements are also useful in discerning whether or not the qubit is actually dead, or whether it was simply far detuned from the resonator.

TODO:

- Explain how qubit's frequency has a cosine dependence on DAC

- Give detailed information on SQUID loop

    - Why does the qubit frequency change in a SQUID loop
    - Sweet-spot

- Mention flux-noise?

    - 1/f noise
    - usually not limiting, as it is very slow
    - This noise can be seen as occasional jumps (every few hours?) It would mean that every few hours the frequency must be recalibrated.

Figures:

- SEM picture of SQUID loop, including flux-bias line

- Figure of 2D resonator scan vs DAC voltage

- Figure of 1D resonator fixed frequency DAC voltage scan

2.1.4 Scanning for qubits

Once the preliminary measurements have been performed that characterize the resonators and provide hints about the whereabouts of the qubit it is time to actually find the qubit.

The measurement to perform in order to find the qubit depends on the amount of detuning between the resonator and qubit, which can be estimated from powersweep measurements. If the amount of detuning is large compared to the coupling strength ($\Delta \gg g$), the system is in the dispersive regime. In this case one commonly performs a two-tone spectroscopy to find the qubit's frequency. If, on the other hand, the detuning is comparable to the coupling strength ($\Delta \sim g$), the qubit and resonator are hybridized, and experience an avoided crossing. In such cases a normal transmission measurement suffices.

If the qubit is flux-tunable, one important question to ask is: at what DAC voltage should the qubit be searched?

One option is to choose zero DAC voltage. In most cases this is alright, but there are cases when this is a bad choice. For instance, trapped magnetic fields during cool-down could position the qubit near the anti-sweet-spot for zero DAC voltage, in which case finding the qubit will be next to impossible.

A better option is to choose a DAC voltage that results in a detuning Δ that is large compared to coupling strength g, such that the system is in the disperisive regime. However, the detuning Δ should not be too high, as it would otherwise result in a negligible dispersive shift χ.The optimum value is usually around a few hundred megahertz, although this is dependent on the device-specific parameters. The detuning can be approximated using powersweeps.

2.1.4.1 Spectroscopy

As was explained in section 2.1.1, in the dispersive regime the resonator experiences a 2χ frequency shift dependent on the state of the qubit. In the case of a resonator capacitively coupled to the feedline, the transmission experiences a dip at the resonator's frequency. This dip will correspondingly shift when the qubit's state is switched. The transmission at the resonator's dip when the qubit is in the ground state will therefore be dependent on the state of the qubit (low when the qubit is in the ground state, high when the qubit is in the excited state). This is the property exploited in a two-tone spectroscopy measurement.

In a two-tone spectroscopy measurement two tones are sent through the feedline.

1. A drive tone with varying frequency ω_{d}.

2. A measurement tone at the resonator's frequency when the qubit is in the ground state.

The transmission through the feedline is measured while the frequency of the drive tone ω_{d} is swept. When the drive frequency ω_{d} is detuned from the qubit's frequency ω_{q}, the drive is off-resonant with respect to the qubit, and so we measure a low transmission due to a dip being present. However, when the drive frequency ω_{d} approaches the qubit's frequency ω_{q}, then the qubit will start to oscillate between its ground and excited state, with a rate dependent on the detuning between the drive frequency ω_{d} and the qubit's frequency ω_{q}. The qubit will therefore have a partial population in the excited state, resulting in a shift of the resonator frequency, dependent on the population in the excited state. This is measured as an increase in transmission.

The minimum linewidth of the qubit using spectroscopy is set by its dephasing time T^2, which can be seen as the uncertainty in its frequency. However, the power of the drive tone causes an additional increase in the linewidth, due to stimulated emission of the qubit. This effect is known as power broadening. This effect can be quite useful for finding qubits, especially when designing high-quality qubits with a very narrow intrinsic linewidth. The optimal power for the drive strength is further dependent on the amount of detuning Δ between the qubit and resonator. The resonator effectively acts as a bandpass filter, centered around the resonator frequency. Therefore, the stronger the detuning, the more the drive tone is suppressed.

The dispersive shift 2χ is also dependent on the amount of detuning Δ between the qubit and resonator. If the detuning Δ is large, the dispersive shift will be very small, and so the difference in transmission will also decrease. Since the resonator has a Lorentzian lineshape, at the resonance frequency this Lorentzian is flat, and so is insensitive to small deviations. To increase the contrast between the on-resonant and off-resonant transmission, it is usually

advantageous to measure at a slight detuning δ away from the resonance frequency, where the transmission slope is high. Since the resonator frequency shifts down when the qubit is excited, it is better to have a positive detuning δ to ensure that the transmission increases as the drive frequence ω_d approaches the qubit frequency ω_q and decreases as it leaves the qubit frequency.

TODO: Spectroscopy section

- Is power broadening really due to stimulated emission?

- Explain optimal RF power

- Is the gradual increase really due to partial population? Is it then an average of the partial population? Or do you get other effects as well?

2.1.4.2 Avoided crossing

When the detuning Δ between the qubit and resonator is not large compared to their coupling strength g, the qubit and resonator experience an avoided crossing. Because all of the qubits in the Muxmon chips are considerably lower in frequency compared to their resonators, the system is always in the dispersive regime, and so the system never approaches the avoided crossing. Nevertheless it is worth mentioning the avoided crossing briefly, as it is a breeding ground for interesting physics.

At the avoided crossing the system is not in the dispersive regime, and so the dispersive Jaynes-Cummings Hamiltonian no longer applies. In this case the resonator and qubit are hybridized, and one can no longer speak of a qubit and resonator as separate entities. Instead, this hybridization results in a so-called quton and phobit.

Avoided crossing info:

- The coupling strength g is the minimum distance be tween the splitting

- From Reed's thesis p.63 explanation of this avoided crossing is given

$$E_0 = -\frac{\hbar\Delta}{2} \tag{2.4}$$

$$E_1 = n\hbar\omega_r \pm \frac{\hbar}{2}\sqrt{4g^2 n + \Delta^2} \tag{2.5}$$

Joining $E_0 + E_1$ results in a qubit approaching a resonator from the top.
When the frequency of the qubit equals that of the resonator, the energy difference reaches a minimum, and is equal to $2g$.

TODO: Avoided crossing

- Explain the quton fobit behaviour near the avoided crossing

- Explain how one can extract coupling from avoided crossing

- Explain that for the Muxmon qubit this effect is not present

- Explain multiple lines near avoided crossing

figures:

- Figure of avoided crossing

TODO:

- Use relatively high source power, results in power broadening

- Mention what to do if qubit is close to or far away from resonator

- Mention the term transmission measurement earlier on.

- Pulsed spectroscopy

2.1.5   Tracking the qubits

For flux-tunable qubits one is usually not interested in finding the frequency at one specific flux value. More important is finding how this frequency changes with varying flux. A naive approach would be to perform a two-dimensional scan of a fixed frequency range versus flux. At a certain flux the qubit crosses the boundary of the chosen frequency window. Every time this happens a new two-dimensional scan has to be performed with an updated frequency window. The larger the chosen frequency window, the less often this has to be updated. On the other hand, choosing a large window also means that a larger portion of the scan is spent not measuring the qubit. There is therefore a trade-off between measurement time and degree of human intervention. Furthermore, the resonator frequency also depends on the amount of detuning. Therefore the frequency of the measurement tone must also be updated every now and then.

As an alternative approach I have created a modified version of the spectroscopy versus flux scan, known as tracked spectroscopy. In this approach after every spectroscopy scan the qubit frequency is extracted through fitting. From the qubit frequencies measured in previous scans the expected frequency at the next flux value is extrapolated. The frequency window of the next spectroscopy scan are then centered around the expected qubit frequency. The qubit is therefore tracked as its frequency changes. The same method is applied to update the resonator frequency.

Tracked spectroscopy has several advantages over the two-dimensional spectroscopy versus flux scans. First of all, since the qubit's frequency follows a smooth curve (see Equation **TODO:** Refer to eqn), the qubit's frequency can be estimated quite accurately. The frequency windows can therefore be narrow. This greatly reduces the measurement time. Secondly, tracked spectroscopy does not need any human intervention, as the frequency window is automatically updated after every spectroscopy scan. Therefore measuring the flux-dependence of the qubit frequencies is an automatized process (provided that the qubit frequency can correctly be extracted).

For more information on the tracked spectroscopy algorithm see appendix C.1.

Improvements

- Avoided crossing

- Variable RF and drive power

TODO:

- Maybe mention possible improvements

Figures:

- Tracked spectroscopy of qubit and resonator

2.1.6   Flux matrix

When a current is passed through a flux-bias line, it is not only the flux through the SQUID of the qubit directly connected to it that is affected. Instead, the flux through SQUIDs of neighbouring qubits are also affected, albeit to a lesser extent. Therefore changing the frequency of one qubit by changing its corresponding flux-bias line current also affects the frequencies of the other flux-tunable qubits on the chip. The effect that the current passing through flux-bias lines has on the frequencies of the different qubits can be decoupled by correcting the flux cross-coupling effects. This is done by implementing a flux matrix.

A flux matrix F is an $n \times n$ matrix, where n is the number of flux-tunable qubits. Each row corresponds to a virtual flux, and can be interpreted as follows: in a row $F_i = [f_{i1}, \ldots, f_{in}]$ each element F_{ij} corresponds to the relative amount by which the flux-bias line of qubit j should be changed, such that only the frequency of qubit i changes, whilst the frequencies of the other qubits remain fixed. This results in n decoupled virtual flux parameters.

Creating a flux matrix is done by first determining for each qubit separately how much every flux-bias line affects its frequency. For a given qubit i this can be found by tuning the qubit away from its sweet-spot using its main flux-bias line, to a point where the slope $\partial f_i / \partial V_i$ of the qubit frequency f_i as a function of DAC voltage V_i is steep. This is the region where we are sensitive to changes in qubit frequency. For the main flux-bias line we already know from tracked spectroscopy what the slope $\partial f_i / \partial V_i$ is at this point. For each of the remaining flux-bias lines we measure the slope $\partial f_i / \partial V_j$ as we vary the DAC voltage V_j and measure the response of the qubit frequency f_i. The slope $\partial f_i / \partial V_j$ is a measure for the amount of flux cross-coupling, which should be considerably less than for the main flux-bias line. Finally dividing all the slopes by the slope $\partial f_i / \partial V_j$ of our main flux-bias line, results in the ratio's of the frequency response of qubit i for each of the flux-bias lines. Performing this measurement for all the qubits results in a matrix M, where each element $M_{ij} = \partial f_i / \partial V_j$ is the normalized frequency response of qubit i when varying the DAC voltage of the flux-bias line corresponding to qubit j. The diagonal elements of matrix M should be equal to one.

Tracked spectroscopy provides accurate information on the DAC voltage corresponding to the sweet-spot of a qubit. The sweet-spot may not lie exactly at zero DAC voltage. It may shift due to magnetic flux being trapped during the cooldown of the fridge. These sweet-spots are usually found in the case where all the remaining flux-bias lines are set to zero DAC voltage. There is a certain combination of DAC voltages $\vec{V}^{ss}$ for which all the qubits are at

their simultaneous sweet-spot. This simultaneous sweet-spot can be found using matrix $\boldsymbol{M}$. We know for each qubit i the DAC voltage V_i^0 corresponding to its sweet-spot. Since $\boldsymbol{M}$ stores the amount by which each flux-bias line affects the flux of any qubit, the qubit i remains at its sweet-spot as long as $\boldsymbol{M}_i \vec{V} = V_i^0$ holds, where $\vec{V}$ is the vector containing the DAC voltages. Therefore the simultaneous sweet-spot $\vec{V}^{ss}$ can be found by solving the set of equations $\boldsymbol{M}\vec{V}^{ss} = \vec{V}^0$, where $\vec{V}^0$ contains the DAC voltages of the individual sweet-spots of the qubits.

The flux matrix $\boldsymbol{F}$ can be found by inverting matrix $\boldsymbol{M}$. As mentioned earlier, each row of matrix $\boldsymbol{F}$ corresponds to the ratio by which the DAC voltages of the flux-bias lines need to be varied, such that the frequency of only one qubit is changed. We may therefore multiply each row by a different constant, as long as the ratio between the elements in each row stays constant. One can normalizing each row such that the main flux-bias line is equal to one. This has the advantage that there is a one-to-one correspondence between DAC voltage and flux, and as a result the tracked spectroscopy will look identical. Additionally, after the normalization each row can be multiplied by a factor such that the virtual flux is equal to the flux quanta present in the SQUID loop. This conversion factor can be obtained by fitting the qubit frequency curve obtained from tracked spectroscopy.

For a given virtual flux vector $\vec{\Phi} = [\phi_1, \ldots \phi_n]$, the corresponding DAC voltages $\vec{V}$ are given by:

$$\vec{V} = \boldsymbol{F}\vec{\Phi} + \vec{V}^{ss} \tag{2.6}$$

By adding the simultaneous sweet-spot DAC voltages $\vec{V}^{ss}$, we obtain the additional property that the sweet-spot of the virtual fluxes is set to zero.

After determining the flux matrix $\boldsymbol{F}$, there will still be some small remaining cross-coupling, which depends on the accuracy of the measurements. The process of creating a flux matrix can then be repeated, but instead of using DAC voltages as the varying parameters to construct matrix $\boldsymbol{M}$, the virtual fluxes should be used. Furthermore, as the cross-coupling is small compared to before, the flux range can be much greater, such that small slopes can be accurately measured. The resulting flux matrix $\boldsymbol{F}_2$ can then simply be multiplied with the first flux matrix $\boldsymbol{F}$ to obtain a more accurate final flux matrix.

2.2 TIME-DOMAIN MEASUREMENTS

2.2.1 Qubit control

So far the measurements described have all dealt with continuous tones being applied and measuring the response in the transmission. These are crude measurements, that are nevertheless able to determine some properties of the qubit and resonator, such as their frequencies. However, to find more detailed properties of the qubits, such as their coherence times, one cannot apply a continuous tone, that drives some incoherent qubit population. Instead well-calibrated pulses are required, which modify the state of the qubit in a precise manner, corresponding to gates being applied to the qubit. These types of measurements are called time-domain measurements, as they require precise pulse timing.

A simple time-domain measurement usually consists of two parts. The first part consists of controlling the qubit. Here pulses are sent which modify the state of the qubit. The second part consists of measuring the state of the qubit. This is done through a readout tone, similar to spectroscopy measurements. This readout tone projects the state of the qubit onto the Z-axis. From the response in the transmission the state of the qubit can be inferred. More complicated experiments may involve some sort of feedback loop, where additional qubit control can be applied depending on the measurement outcome. These measurements require the qubit readout to be quantum non-demolition, i.e. the state of the qubit is not destroyed in the process of qubit readout. This usually involves extremely low-noise amplification, such as through a Josephson parametric amplifier. Feedback measurements are not performed in this experiment, and are therefore beyond the scope of this thesis.

Qubit pulses usually have a Gaussian shape. These pulses can be generated by modulating a carrier signal from an RF generator, and is commonly done using an Arbitrary Waveform Generator (AWG). For the Muxmon experiment the Tektronix AWG5014 is used, which has four channels, each of which can control its voltage output at the nanosecond scale. It further has eight marker channels, which can be used to trigger devices, such as RF generators and the Duplexer. The carrier signal is sent through the LO port of the mixer, and an AWG channel is connected to the IF port of the mixer. The ouput at the RF port of the mixer is the modulated signal, the amplitude of which depends on the amplitude of the AWG channel output.

For IQ mixers it is also possible to modulate both quadratures of the carrier signal independently, using two AWG channels. This allows for single sideband modulation, which is done by convoluting the pulses of the I and Q quadrature channels with a sine and cosine respectively. The sideband modulation frequency ω_{sb} of these sinusoidal functions is the amount by which the carrier signal is shifted. Single sideband modulation has the advantage that the carrier frequency ω_c is shifted away from mixer leakage, which would otherwise cause a slight continuous rotation of the qubit. For more information on mixer leakage, see section 3.4.

The length of the pulse is an important consideration. Shorter pulses allow for more qubit operations within its coherence time. On the other hand, the shorter a pulse is in time, the larger its frequency spectrum will be. At a certain point the spectrum will be so broad that there will be a nonnegligible signal at the qubit's excited-state to second excited-state transtion frequency. This will cause leakage to the second excited-state, thereby leaving the two-state Hilbert space. Furthermore, the finite resolution of the AWG causes the pulses to be discretized, resulting in the pulses being slightly distorted. The shorter the length of the pulse, the more discretization, and therefore distortion, will occur. This can cause further leakage to the second excited-state. It is therefore desirable to have a bandwidth, which is the inverse of the width σ of the Gaussian pulse, that is small compared to the anharmonicity of the qubit.

A second pulse, known as the Derivative Removal by Adiabatic Gate (DRAG) pulse [8], can be applied along with the main pulse, to reduce the amount of leakage. The DRAG pulse is the derivative of the main Gaussian pulse, and adiabaticaly populates the second excited state during the pulse, and subsequently withdraws this population back to the two-state Hilbert space. Using the DRAG pulse can reduce the amount of leakage by orders of magnitude.

TODO:

- Explain more on Z projection

- Explain more on non-demolition.

- Signal quadrature determines the rotation angle

- Mention that AWG channel amplitude must not be too high, and that attenuation should be used to avoid spurious resonant modes

- Refer to Noise chapter for more information on single sideband modulation?

- Mention that amount of rotation depends on time duration, refer to Reed's thesis

Questions:

- Are both quadratures modulated independently in IQ mixers?

- Why use sideband modulation?

- Why are Gaussian pulses used?

Figures:

- Gaussian pulse with derivative

2.2.2   Calibrating drive amplitude

Performing gates on qubits requires knowledge of the parameters that define the pulse, such as the amplitude, phase, and pulse duration. The phase determines the axis along which the qubit is rotated. The duration and amplitude of the pulse determine the rotation angle. To rotate the qubit by a specific angle, either the pulse duration can be varied, keeping the amplitude fixed, or the pulse amplitude can be varied, keeping the pulse duration fixed. Both methods have advantages and disadvantages. Varying the pulse duration ensures that the maximum amplitude is roughly fixed, regardless of the rotation angle. On the other hand, pulses with a small rotation angle have a very small duration, and so their bandwidth will be large, which may lead to increased leakage. Varying the amplitude, on the other hand, ensures that pulses applied to multiple qubits end simultaneously, and so it is more natural to speak of a pulse clock cycle. In the measurements for this thesis the amplitude is varied, whilst the pulse duration is kept fixed.

Determining the correct amplitude for qubit gates is commonly performed using a Rabi measurement. In this measurement the amplitude of a pulse with rotation along the X-axis is varied monotonically. The pulse will cause the qubit to rotate at a Rabi rate Ω_R, which depends on the pulse amplitude.

After application of a pulse with Rabi rate Ω_R and duration τ, the wavefunction will be in state $|\psi\rangle = \cos\left(\frac{\Omega_R}{2}\tau\right)|0\rangle + \sin\left(\frac{\Omega_R}{2}\tau\right)|1\rangle$. After a measurement the qubit will be in the excited state with probability $\sin^2\left(\frac{\Omega_R}{2}\tau\right)$ [11]. The Rabi rate Ω_R is proportional to the pulse amplitude.

In a Rabi measurement the amplitude is swept monotonically from a negative value to a positive value. The result should look like a cosine, as shown in Figure **TODO**. The center of this cosine is where the amplitude is zero, and therefore corresponds to the ground-state of the qubit. At the other peaks, where the deviation from the ground-state is the largest, the qubit is in the excited-state. The amplitude of the left peak corresponds to a negative pi-pulse, and the right peak to a positive pi-pulse. Usually the amplitude step between successive segments is tuned such that the excited-state peaks are at specific segments.
    Questions:

- How does the rotation angle depend on the amplitude?

TODO:

- time variation or amplitude variation

- Refer to equation showing that rotation depends on time duration (Reed's thesis)

2.2.3   Qubit decoherence

2.2.3.1   Qubit relaxation

Once a pi-pulse has been tuned it is possible to excite the qubit. However, once the qubit is excited, it will not remain so indefinitely. Instead, the excitation will slowly leak away to different relaxation sources, some of which have been discussed in 0.3. These sources of relaxation lead to an exponential decay of the qubit's excitation, with a relaxation time T_1. A typical measurement to characterize the relaxation time T_1 is performed by first applying a pi-pulse, and the waiting for a monotonically increasing wait time τ, after which the state of the qubit is measured.
    relaxation time T_1,

- Purcell limit

2.2.3.2   Qubit dephasing

Spectroscopy provides an estimate for the frequency of the qubit. However, even with pulsed spectroscopy, the accuracy is limited to roughly a megahertz. When the frequency of the driving tone ω_d is different from the qubit frequency ω_q, the qubit will precess around the Z-axis with a frequency equal to the Rabi rate $\Omega_R = \omega_d - \omega_q$. This property is exploited in a Ramsey measurement, where the qubit frequency can be inferred from the precession rate. A Ramsey measurement is performed by first applying a $X_{\pi/2}$ pulse, after which the qubit lies on the equator of the Bloch sphere. The state of the qubit then starts to precess around the equator, with a rate determined by the amount of detuning Δ. After a certain wait time τ, a second $X_{\pi/2}$ pulse is applied to the qubit.
    At the moment we ignore effects such as decoherence and gate errors. The first pulse results in the qubit being at the equator. If there were no precession, the result of the second pulse is that the qubit is in its excited-state. However, any detuning Δ causes the state of the

qubit to deviate from the excited-state. In fact, after half a period the second pulse results in the qubit being in its ground-state. After one full period, however, the qubit has returned to its original position on the equator, and so the second pulse will result yet again in the qubit being in its excited-state. In a Ramsey measurement the final state of the qubit is measured as the wait time τ between the two pulses is monotonically increased. The result should exhibit an oscillatory behaviour, the frequency of which being equal to the Rabi rate Ω_R.

In reality however, the qubit does suffer from decoherence. Especially phase noise, characterized by the dephasing time T_2^*, is noticeable in a Ramsey measurement. Phase noise can be seen as fluctuations in the qubit frequency. The dephasing time T_2^* has an upper bound equal to $2\,T_1$, but can decrease significantly due to other sources of phase noise, such as charge noise, fluctuating cavity photon number, and flux noise for flux-tunable qubits [13, p. 126]. The result of dephasing is that the oscillations will decrease in amplitude as the wait time is increased. For a Ramsey measurement the excited-state population P_1 as a function of wait time is given by:

$$P_1(t) = e^{t/T_2^*} * \cos(2\pi\,\Omega_R\,t) + 1/2 \qquad (2.7)$$

Usually in a Ramsey measurement artificial detunining is added to the pulse, such that if there were no real detuning, one would see around three to four oscillations. There are several reasons for this artificial detuning. One reason is that estimating the detuning using Equation 2.7 is more accurate once there are several oscillations present. Another reason is that if the real detuning is reasonably small compared to the artificial detuning, it is possible to estimate if the qubit's frequency is higher or lower than the drive, as this would result in a higher or lower oscillation frequency.

- coherence time, drive amplitude

- Accuracy of calibrating the frequency depends on the dephasing time T_2^*

- Two T_2^* values, one for exponential? noise, one for Gaussian noise

- dephasing is maximum twice relaxation

Questions:

- How is the Rabi rate Ω_R related to the detuning?

- Where does exponential noise and Gaussian noise come from? As I understand it Gaussian noise is due to flux

- Is T_1 not noticeable in a Ramsey measurement?

- Dephasing results in a mixed state, and therefore shrinks towards the Z-axis on the Bloch sphere?

TODO:

- Remove parts about frequency tuning, add that in calibration section

Figures:

- Ramsey measurement

- T_2^* vs. frequency?

2.2.3.3   Echo measurement

The dephasing time T_2^* is a combination of several different phase noise sources. Some of these sources produces high frequency (fast) noise, whilst others produce low frequency (slow) noise. It is possible to distinguish these two effects by performing a second dephasing measurements that filters out slow noise, called an Echo measurement.

An Echo measurement is quite similar to a Ramsey measurements, where two $X_{\pi/2}$ pulses are applied, separated by a wait time τ. The difference is that in the middle of this wait time, at $\tau/2$, an additional refocusing X_π pulse is sent. This has the effect that the state of the qubit is essentially flipped on the Bloch sphere around the X-axis. Any slow phase noise, which we can view to be quasi-static, is thereby cancelled. Fast phase noise, however, will vary considerably during the wait time τ, and so will still cause dephasing. In the absence of decoherence, the final state of the qubit is the ground-state, which is in contrast to a Ramsey measurement, where the final state is the excited-state.

An Echo measurement is performed by monotonically increasing the wait-time τ, whilst keeping the three pulses relative to the wait time τ fixed. The result is similar to a Ramsey measurement, showing an exponential decay, with corresponding Echo dephasing time T_2^E. This value should be higher or equal to the dephasing time T_2^*. The refocusing pulse has the additional effect that any precession due to detuning is also cancelled. This inhibits the oscillatory behaviour that is present in Ramsey measurements. To be able to better estimate the Echo dephasing time T_2^E, the phase of the final $X_{\pi/2}$ pulse is monotonically shifted, such that the result is an oscillation in qubit state.

There are more complicated Echo sequences, involving multiple refocusing pulses. By placing these at specific times the different frequency contributions of the phase noise can be characterized. Furthermore, by repeatedly applying a refocusing pulse, the state of the qubit can be preserved much longer than the limit imposed by T_2^*.

- T_2^E Should be larger than T_2^*

Figures:

- Echo measurement.

2.2.4   Measuring single shots

* [ ]Explanation of gates * [ ]Motzoi parameter * [ ]Calibrating drive amplitude using Rabi * [ ]Calibrating frequency using Ramsey * * Conflict with next section on accurate tune-up?
    * [ ]Measuring decoherence * * Relaxation * * T1 measurement
    * Dephasing * * Ramsey measurement (all noise) * Echo measurement (fast noise)

* Change with frequency * * Ideally T2 is 2*T1 * T2 rapidly decreases as moving away from sweet-spot
* [ ]Single-shot measurements * * Able to see relaxation and thermal excitation
* [ ]Second excited state * * Similar to three-tone spectroscopy * Nearly identical position in IQ-plane as first excited state, but less relaxation into ground state * Since time-trace is averaged, the final signal is therefore further away from the ground state in the IQ-plane
* [ ]Crosstalk / cross-coupling?

Chapter 3

Calibration routines

Chapter 4

Randomized benchmarking

4.1 SECOND EXCITED STATE

Appendices

Appendix A

Noise

When performing measurements one is faced with the reality that no component is ideal. When a signal passes through the different parts of a set-up, noise is constantly being added. Noise is the term given for all the random fluctuations that are added to the signal. These fluctuations are the cumulative result of several noise source contributions.

Thermal noise is one of the most common sources of noise. It is the result of the random thermal fluctuations of electrons. It is an example of frequency-independent noise, also known as white noise. Noise sources can also be frequency-dependent, such as TLS, as discussed in Chapter **??**. This is an example of $1/f$-noise: the amount of noise added increases with decreasing frequency. In fact, truly frequency-independent noise does not exist, as even white noise has been observed to decrease at extremely high frequencies ($\sim 10^{15}$ Hz). At these frequencies a quantum correction needs to be added [14, p. 50].

When performing measurements one important question to ask is how much noise is being contributed to the signal. In this chapter a model is presented for the general set-up used for measuring superconducting resonators and qubits. Using this model it is possible to characterize the amount of noise by determining its associated noise temperature. Finally, this model is applied to the set-up used to characterize the resonators presented in Chapter **??**.

A.1 CHARACTERIZING NOISE

A.1.1 Circuit representations

There are two circuit representations in which we can depict a system with a noise contribution: The Thévenin representation, and the Norton representation. In the Thévenin representation we can model the system as a voltage source, and the noise added to the system is a noise voltage source connected in series. In the Norton representation the system is a current source and the noise added is a noise current source connected in parallel to the current source. These two representations are identical and can be converted to each other. In this section we will adopt the Thevénin representation, and so the signal will be a voltage source combined in series with a noise voltage source.

Assuming the signal to be at a fixed frequency ω and amplitude A, the combined voltage

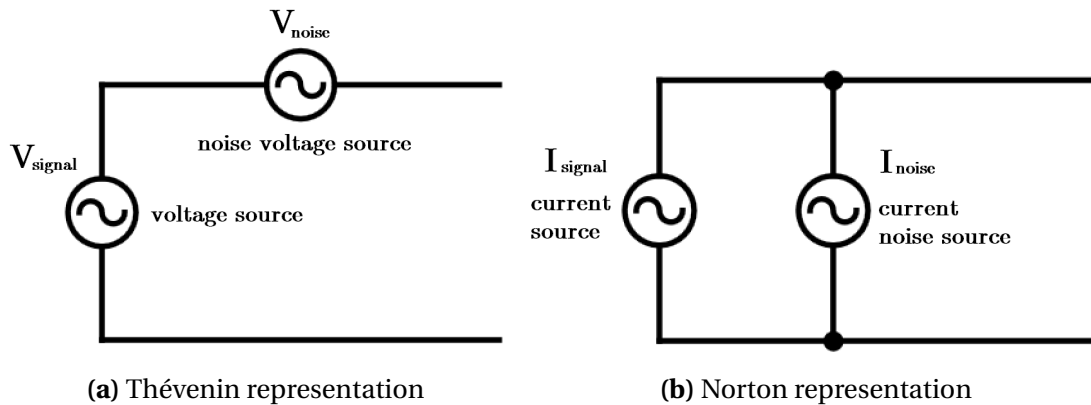**(a)** Thévenin representation   **(b)** Norton representation

Figure A.1: Two equivalent representations of a system containing noise. Panel **(a)** shows the Thévenin representation, in which a noiseless voltage source is connected in series with a noise voltage source. Panel **(b)** shows the Norton representation, in which a noiseless current source is connected in parallel with a noise current source.

$v(t)$ is then given by:

$$v(t) = v_{\text{signal}}(t) + v_{\text{noise}}(t) = A\cos\omega t + v_{\text{n}}(t) \tag{A.1}$$

Note that the mean value of the noise voltage $\overline{v_{\text{n}}}$ is equal to zero. The amount of noise can be quantified by the root-mean square noise voltage $v_{\text{n}}^{\text{rms}}$:

$$v_{\text{n}}^{\text{rms}} = \sqrt{\overline{v^2} - \overline{v}^2} = \sqrt{\overline{v_{\text{n}}^2}} \tag{A.2}$$

A.1.2   Noise power spectral density

One way of quantifying the noise of the system is through the noise power spectral density $S(f)$, which is the distribution of noise power per unit bandwidth as a function of frequency. For the Thévenin representation, the noise spectral density is defined in terms of voltage. When the only noise in the system is white noise, the spectral density is independent of frequency. It is then given by:

$$S = \frac{\overline{v_{\text{n}}^2}}{\Delta f} \qquad\qquad [\text{V}^2/\text{Hz}] \tag{A.3}$$

In this equation Δf is the noise bandwidth. This is the bandwidth over which the noise is measured.
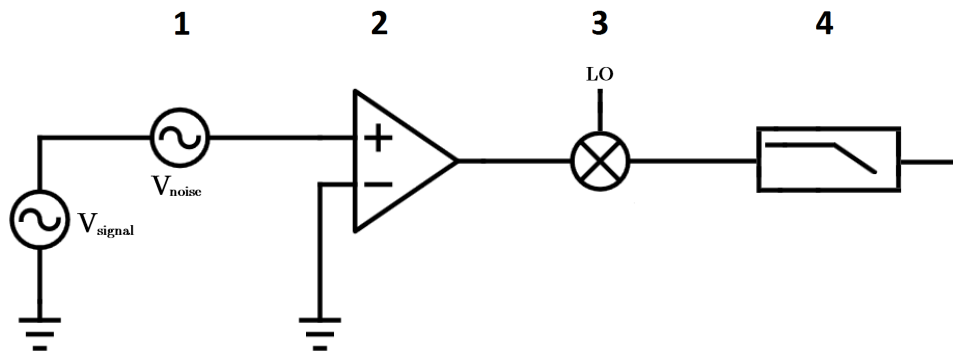
Figure A.2: Schematic representation of the measurement set-up including a noise source.

A.2   THE MODEL

As shown in the schematic in Figure A.2, we can model our set-up as a combination of four elements:

1. A noise source.

2. An amplifier to amplify the weak signal exiting the fridge.

3. A mixer to downconvert the signal.

4. A low-pass filter to remove unwanted high-frequency signal.

A.2.1   Noise source

Using the Thévenin model, we can approximate the components up to the first amplifier in the fridge as a voltage source, with a noise voltage source connected in series.

   We can include the noise added by the amplifier in the noise voltage source, in which case we assume the amplifier to be ideal. Furthermore, we assume the signal to be amplified sufficiently, such that the mixer and low-pass filter add a negligible amount of noise. We also ignore effect such as mixer leakage. With these assumptions all of the noise is originated from the noise voltage source.

   We can associate an effective noise temperature to the noise voltage source. The noise temperature is defined as the temperature at which a resistor would produce an equal amount of noise. Note that, since we are comparing the system to a resistor, the noise needs to have an (approximately) white spectrum.

   According to Nyquist's theorem [14, p. 47], if the system experiences white noise, and is in thermal equilibrium, the root-mean square noise voltage v_n^{rms} is given by:

$$v_n^{rms} = \sqrt{\overline{v_n^2}} = 4k_B T R \Delta f \tag{A.4}$$

In this equation Δf is the bandwidth over which the noise is integrated, k_B is the Boltzmann constant, T is the noise temperature of the noise source, and R is the impedance of

the system. We see that the noise added depends linearly on the bandwidth over which is integrated.

Combining Equations A.3 and A.4, the noise power spectral density S_{v_n} can be rewritten as:

$$S = \frac{\overline{v_n^2}}{\Delta f} = 4k_B T R \tag{A.5}$$

A.2.2 Amplification

During the amplification stage both the signal and the noise is amplified by the same amount. This amount of amplification is determined by the gain G, which is defined as the ratio between the output voltage and the input voltage:

$$G = \frac{v_{out}}{v_{in}} \tag{A.6}$$

According to the maximum power transfer theorem, the maximum power transfer between a source and load occurs when the impedances of source and load are matched, in which case half of the power is transferred. From this it follows that in the amplification process half of the signal is dissipated. However, as G is defined as the ratio between v_{out} and v_{in} (Equation A.6), the factor $\frac{1}{2}$ is included in G.

During amplification not only the signal is amplified with gain G: the noise is amplified by the same amount. Defining the noise power spectral density before amplification as S^{in}, and after amplification as S^{out}, the following relation holds:

$$S^{out} = G^2 S^{in} = G^2 4k_B T R \tag{A.7}$$

Note that in Equation A.7, the gain G is squared. This is due to the fact that the noise power spectral density depends quadratically on the root-mean square noise voltage (Equation A.3).

In our actual set-up the amplification occurs in multiple stages. Aside from amplifying the signal and its noise, at each stage additional noise, originating from the amplifier itself, is added as well. This added noise is then also amplified in the next amplification stage. Therefore it is always best to have the amplifier with highest gain and lowest noise temperature as the first amplifier in the chain. For more information see Friis formula [14, p. 103].

A.2.3 Downconversion

After amplification the frequency ω of the signal is still in the GHz range. In homodyne or heterodyne detection the signal is downconverted to DC (homodyne) or to a lower frequency (heterodyne), such that it can be measured more easily. To downconvert the signal, it is mixed in a mixer with a local oscillator (LO) signal having the same frequency ω (homodyne) or a slightly higher frequency $\omega + \Delta\omega$ (heterodyne). The mixer effectively multiplies the two signals. If the signal exiting the amplifier is given by $v(t) = A\cos\omega t$, then, ignoring a possible phase difference, the signal at the output of the mixer is given by:

$$v(t) \cdot \cos \omega t = A \cos \omega t \cdot \cos (\omega + \Delta \omega) t$$

$$= \frac{1}{2} A \left[\cos (2\omega + \Delta \omega) t + \cos \Delta \omega t \right] \tag{A.8}$$

As can be seen from Equation A.8, the output signal contains both the sum and the difference of the two signals. However, as the sum of both frequencies is in the GHz range, it can be filtered out using a low-pass filter, leaving only the downconverted signal, which is the result of the difference between the two frequencies. Note that the amplitude of the signal is reduced by a factor two. The noise amplitude is also reduced by a factor 2. Furthermore, in the case of a homodyne set-up, the difference signal is simply a DC signal ($\Delta \omega = 0$), while in the case of heterodyne the signal still contains a slow frequency $\Delta \omega$. For simplification we assume our set-up to be a homodyne set-up, although the result is similar in the case of a heterodyne set-up.

A.2.4   Low-pass filtering

In the case of homodyne detection the signal at the frequency of interest is downconverted to DC. However, the signal at other frequencies have not disappeared; in the mixer these have also shifted in frequency. Since the signal of interest is at DC, a low-pass filter can be used to filter out signal above a certain frequency.

The frequency above which a low-pass filter will filter out the signal is defined by its cut-off frequency f_c. The cut-off frequency f_c is the frequency at which the signal is attenuated by 3 dB. For first-order low-pass filters the noise bandwidth Δf is related to the filter cut-off frequency f_c by [14, p. 81]:

$$\Delta f = \frac{\pi}{2} f_c \tag{A.9}$$

A.3   NOISE TEMPERATURE

In the previous sections the influence of each of the components on the signal and on the noise has been analyzed. Using this information it is possible to determine the signal-to-noise ratio (SNR), which is the ratio between the average power of the signal and the average power of the noise. The SNR is a measure for how well a signal can be separated from the noise, and is given by:

$$\mathrm{SNR} = \frac{\overline{v_{\mathrm{out}}}^2}{\overline{v_n^2}} = \frac{1/4 \, G^2 \, \overline{v_{\mathrm{in}}}^2}{S_{v_n}^{\mathrm{out}} \, \Delta f}$$

$$= \frac{1/4 \, G^2 \, \overline{v_{\mathrm{in}}}^2}{G^2 \, S_{v_n}^{\mathrm{in}} \, \frac{\pi}{2} \, f_c}$$

$$= \frac{\overline{v_{\mathrm{in}}}^2}{2 \, \pi \, k_B \, T \, R \, f_c} \tag{A.10}$$

Note that the factor 1/4 is because the amplitude is lowered by a factor of 2 due to mixing. Equation A.10 can be rewritten such that we have an expression for the noise temperature of the system:

$$T = \frac{\overline{v_{\text{in}}}^2}{2 \pi k_B R f_{\text{c}} \text{SNR}} \tag{A.11}$$
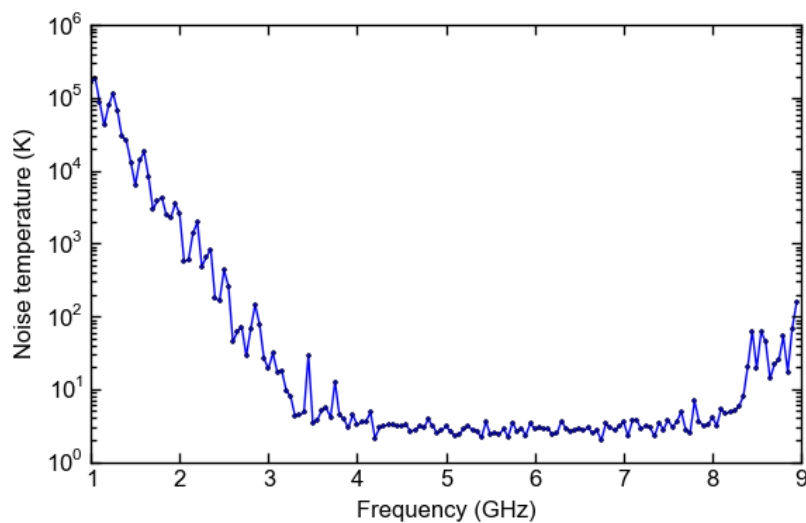
A.4 RESULTS

Figure A.3: Noise temperature versus frequency. The noise temperature has been calculated for 160 frequencies in the range 1–9 GHz. For each frequency 2001 points were measured, from which the signal, noise, SNR, and noise temperature was determined. Measurements were performed at an input power of −113 dBm and an IF bandwidth of Δf =300 Hz.

Using the Rhode & Schwarz ZVM vector network analyzer, The transmission has been measured for 160 equidistant frequencies in the range 1–9 GHz. For each frequency a total of 2001 points was measured with an IF bandwidth Δf = 300 Hz. From these measurements the signal-to-noise ratio has been determined for each frequency. With knowledge of the SNR, the noise temperature has then been determined as a function of frequency using Equation A.11 . The result is shown in Figure A.3.

From Figure A.3 it is clear that the noise temperature is highly temperature-dependent. In the frequency range 4–8 GHz the noise temperature is quite low, never reaching above 10 K. This is exactly the bandwidth of the cryogenic low-noise amplifier by Low Noise Factory, which is the first amplifier in the amplification chain. From the specifications of the amplifier, the noise temperature of the amplifier has been calculated at an ambient temperature of 8 K, and equals roughly 4 K for the entire bandwidth. Comparing the amplifier specifications with Figure A.3, it is likely that in the frequency range 4–8 GHz the first amplifier is the component contributing most to the total noise temperature.

Outside the 4–8 GHz frequency band, however, the noise temperature rapidly increases. This is partly due to the frequency lying outside of the bandwidth of the amplifier, in which case the amplification will be lower. However, this is not an adequate explanation for the fact that the noise temperature increases to several hundred thousand Kelvin. The reason for this unrealistic noise temperature is that in our model we did not take into account the noise added by components after the amplifier. While the gain of the amplifier decreases outside its bandwidth, the components after the amplification will still add the same amount of noise. When the gain decreases by a significant amount, the relative contribution of these post-amplification noise sources will increase. Furthermore the assumption that the noise spectrum is white is no longer correct at low frequencies, where $1/f$ noise starts to contribute.
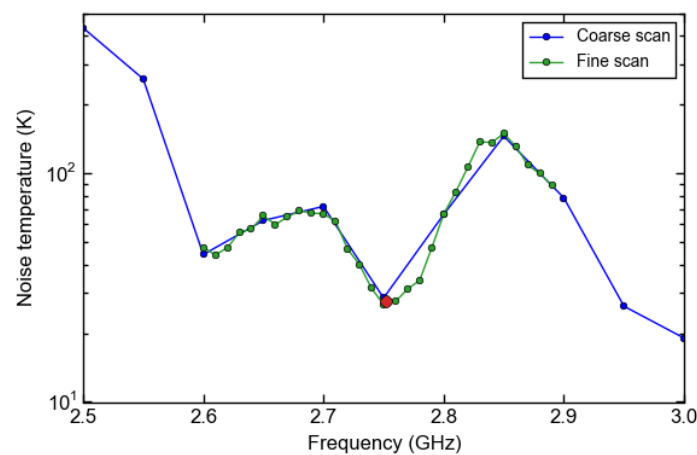

Figure A.4: Detailed scan of noise temperature versus frequency in the range 2.6–2.9 GHz. The resonator with f_0 =2.75 GHz (red dot) seems to reside at a local minimum of the noise temperature.

From Figure A.3 it can be seen that the noise temperature can vary by a large amount between consecutive points. To determine whether this variation is due to a large uncertainty, or due to the noise temperature actually fluctuating strongly with varying frequency, a more detailed scan has been performed in the frequency region 2.6–2.9 GHz, in which one resonator has a resonance frequency. The result is shown in Figure A.4. As the curve of the detailed scan follows the curve of the coarse scan pretty closely, it can be concluded that the noise temperature of the system in fact fluctuates quite strongly with varying frequency.

Another point of interest is that the resonance frequency of the resonator lies near the local minimum of the noise temperature in that region. This is quite a stroke of luck, as a slightly higher or lower frequency would have resulted in a much higher noise temperature.

A.5 CONCLUSION AND FUTURE WORK

The noise temperature gives us an estimate of the noise added to the system. It has been shown that the noise temperature can fluctuate strongly with varying frequency. In the model used to estimate the noise temperature it has been shown that outside the bandwidth of the

amplifier the model breaks down. At this point the noise added by the components after the amplification, and indeed even the amplifiers themselves, needs to be taken into account to obtain accurate estimates of the noise temperature.

However, even outside of the bandwidth of the amplifier, there are frequency regions in which the noise temperature may still be acceptable. It is therefore a good idea to initially perform measurements of the noise temperature of the set-up. This will give an indication of the signal-to-noise ratio, from which accurate estimates can be made as to what the amount of measurement time is needed to obtain a desired SNR.

The noise temperature measurements were performed using the Rhode & Schwarz ZVM vector network analyzer. It would be interesting to see how other measurement set-ups would compare to the vector network analyzer. One interesting candidate would be a heterodyne detector. However, as the vector network analyzer can also measure phase, a fair comparison would also require the heterodyne detector to be able to measure the phase. This heterodyne detector is currently being set up, and will hopefully soon yield interesting results.

Aside from only comparing the noise temperature, other properties are also important when comparing two set-ups. One of these is the duty cycle, which is the percentage of time acually spent measuring. For the vector network analyser the duty cycle seems to be around 50%, provided that a single measurement sweep takes at least a few seconds. Other set-ups may therefore offer an improvement in the duty cycle. Furthermore, properties such as phase stability and uncertainty would also be interesting to compare.

Another interesting measurement would be to see if the noise temperature as a function of frequency remains the same in future cooldowns, and for different samples.

Appendix B

Additional notes

B.1 QUBIT CHARACTERIZATION

B.1.1 Part I: Continuous-wave measurements

B.1.1.1 Powersweep

- If the resonator seems to disappear after the transition from dressed frequency to bare frequency (or vice versa), this is likely due to the qubit being extremely close to the resonator, and so the frequency shift is large.

B.1.1.2 Spectroscopy

- If the deviation in transmission becomes less due to more detuning, increasing the power can also increase the contrast.

B.1.2 Part I: Time-domain measurements

B.1.2.1 AllXY

TODO:

- Table of AllXY pulses

Appendix C

Algorithms

C.1 TRACKED SPECTROSCOPY

- Information may lie in amplitude or in phase, or in a combination of the two. For most accurate measure, calculate distance from ground state.

C.2 PEAK FINDING

C.2.1 Normal peak finder

C.2.2 Derivative peak finder

C.3 COMPILED RB?

Bibliography

[1] R Barends, HL Hortensius, T Zijlstra, JJA Baselmans, SJC Yates, JR Gao, and TM Klapwijk. Contribution of dielectrics to frequency and noise of nbtin superconducting resonators. *Applied Physics Letters*, 92(22):223502, 2008.

[2] Rami Barends. *Photon-detecting superconducting resonators.* PhD thesis, Delft University of Technology, 2009.

[3] A. Bruno, G. de Lange, K. van der Enden, S. Asaad, N. Langford, and L. DiCarlo. Extending single-photon relaxation time in superconducting resonators by surface treatment and deep etching of silicon substrates. Unpublished.

[4] Jiansong Gao, Miguel Daal, Anastasios Vayonakis, Shwetank Kumar, Jonas Zmuidzinas, Bernard Sadoulet, Benjamin A Mazin, Peter K Day, and Henry G Leduc. Experimental evidence for a surface distribution of two-level systems in superconducting lithographed microwave resonators. *Applied Physics Letters*, 92(15):152505–152505, 2008.

[5] Kurtis L. Geerlings. *Improving Coherence of Superconducting Qubits and Resonators.* PhD thesis, Yale University, 2013.

[6] John M Martinis and A Megrant. Ucsb final report for the csq program: Review of decoherence and materials physics for superconducting qubits. *arXiv preprint arXiv:1410.5793*, 2014.

[7] Benjamin A. Mazin. *Microwave Kinetic Inductance Detectors.* PhD thesis, California Institute of Technology, 2004.

[8] F Motzoi, JM Gambetta, P Rebentrost, and Frank K Wilhelm. Simple pulses for elimination of leakage in weakly nonlinear qubits. *Physical review letters*, 103(11):110501, 2009.

[9] I Nsanzineza and BLT Plourde. Trapping a single vortex and reducing quasiparticles in a superconducting resonator. *arXiv preprint arXiv:1405.0256*, 2014.

[10] Britton Plourde, C Song, TW Heitmann, MP DeFeo, and Kang Yu. Microwave response of vortices in superconducting thin films of re and al. 2009.

[11] Matthew D. Reed. *Entanglement and Quantum Error Correction with Superconducting Qubits, year =.* PhD thesis.

[12] Jeremy M Sage, Vladimir Bolkhovsky, William D Oliver, Benjamin Turek, and Paul B Welander. Study of loss in superconducting coplanar waveguide resonators. *Journal of Applied Physics*, 109(6):063915, 2011.

[13] Adam P. Sears. *Extending Coherence in Superconducting Qubits: from microseconds to milliseconds*. PhD thesis, Yale University, 2013.

[14] Gabriel Vasilescu. *Electronic noise and interfering signals: principles and applications*. Springer, 2006.

[15] J Wenner, R Barends, RC Bialczak, Yu Chen, J Kelly, Erik Lucero, Matteo Mariantoni, A Megrant, PJJ OâĂŹMalley, D Sank, et al. Surface loss simulations of superconducting coplanar waveguide resonators. *Applied Physics Letters*, 99(11):113513, 2011.